applied optics

Optimization of adiabatic microring resonators with few-mode and high-Q resonances

Ruifei Li, Linjie Zhou,* Jingya Xie, Anbang Xie, and Jianping Chen

State Key Laboratory of Advanced Optical Communication Systems and Networks, Department of Electronic Engineering, Shanghai Jiao Tong University, Shanghai 200240, China
**Corresponding author: ljzhou@sjtu.edu.cn*

Received 11 September 2015; revised 25 October 2015; accepted 4 November 2015; posted 4 November 2015 (Doc. ID 249975); published 30 November 2015

We present the theoretical analysis and experimental demonstration of adiabatic microring resonators. The resonators are halfway between microdisk and microring preserving the good properties of both the microdisk (high *Q*-factor) and the microring (internal mode rejection). Device modeling based on the coupled-mode theory suggests that both the internal and external decay rates should be low in order to obtain high-*Q* and high extinction ratio resonances. The internal decay is modal-order-dependent and significantly affected by the adiabatic tapering rate of the ring waveguide. The external delay is determined by the modal effective index difference between the bus and ring waveguides at the coupling point under a fixed gap. Upon optimization of the resonator system, two resonance modes in the measured device are measured with one possessing a high *Q*-factor.

OCIS codes: (140.3948) Microcavity devices; (140.4780) Optical resonators; (230.3120) Integrated optics devices; (230.5750) Resonators; (230.7390) Waveguides, planar.

http://dx.doi.org/10.1364/AO.54.010207

1. INTRODUCTION

Microring resonators are one of the main building blocks in silicon photonics due to their simple structure, compact size, and agile functionality. They have been regarded as attractive candidates to build ultracompact optical filters, switches, modulators, biochemical sensors, lasers, and so on [1–8]. The quality factor (*Q*-factor) is a key parameter to describe the sharpness of the resonance spectral line shape. A high *Q*-factor is frequently pursued in a lot of applications requiring a narrow filtering window [9–11] or a strong resonance enhancement effect [12]. Silicon microring resonators fabricated by the routine photolithography and reactive ion etch process without special surface treatment typically have a medium *Q*-factor of around 10^4 [13,14]. The *Q*-factor is primarily determined by the scattering loss induced by the roughness on the two waveguide sidewalls. Therefore, its *Q*-factor is intrinsically lower than that of the microdisk resonator with no inner sidewall [15]. However, the microdisk resonator possesses multiple whispering gallery modes (WGMs), which narrows down the available spectral window for certain applications. For instance, in wavelength division multiplexing [16,17], a single channel needs to be filtered out without perturbing others. Therefore, it is highly desirable to suppress higher-order modes and selectively excite the lowest few-modes in microdisk resonators, which has attracted much attention in recent years [18–20].

One of the compromise solutions is to use a microdonut resonator [10,21,22] in which the circular waveguide has a wider uniform width so that the fundamental mode does not interact with the inner sidewall significantly. It has a resonance *Q*-factor comparable with the microdisk and the higher-order modes are cut off. The circular waveguide width should not be too wide in order to maintain few-mode resonances. On the other hand, the waveguide also should not be too narrow, if active electric-optic or thermo-optic tuners are to be integrated directly in the waveguide. A better approach, therefore, is to design a nonuniform circular waveguide which has a narrow width at the coupling point and is adiabatically widened to a larger width at the opposite point [23]. The narrow width facilitates efficient coupling with the bus waveguide while the wide waveguide can provide enough space for electrical or thermal contact.

For a fixed resonator size, i.e., constant outer radius, there are two geometric parameters that affect the resonance property, the inner radius and its position with respect to the outer one. In this paper, we explore the effect of these two parameters on the resonance *Q*-factor and extinction ratio (ER) in the adiabatic microring resonator coupled with a single straight bus waveguide.

2. DEVICE STRUCTURE AND MODELING

Figure 1(a) shows the schematic of the adiabatic microring resonator coupled with a straight bus waveguide. The adiabatic

microring resonator is formed by a disk (radius R) with a hole etched inside (radius r). The center of the inner hole is shifted so that the width of the ring waveguide changes adiabatically from d_1 at the coupling point to d_2 on the opposite.

Figure 1(b) shows the microscope image of a typical adiabatic microring resonator. The silicon waveguide has a height of 220 with a 60 nm slab. The width of the bus waveguide is 0.35 μm and the gap size between the bus waveguide and the microring resonator is 0.2 μm.

We first adopt the temporal coupled-mode theory to model the adiabatic microring resonator. The change rate of the energy in the resonator is given by [24]

$$\frac{da}{dt} = \left(j\omega_0 - \frac{1}{\tau_l} - \frac{1}{\tau_e}\right)a - j\sqrt{\frac{2}{\tau_e}}s_i, \tag{1}$$

where $|a|^2$ is the total energy in the resonator, ω_0 is the resonance angular frequency, $1/\tau_l$ is the intrinsic decay rate due to loss in cavity, $1/\tau_e$ is the external decay rate due to output coupling to the bus waveguide, and S_i is the incident wave. The total decay rate is $1/\tau = 1/\tau_l + 1/\tau_e$. The transmitted wave is the summation of the incident wave and the output coupled wave from the resonator, given by

$$s_t = s_i - j\sqrt{\frac{2}{\tau_e}}a. \tag{2}$$

The optical power coupling coefficient between the bus waveguide and the ring waveguide κ^2 is related to the external delay rate as $\kappa^2 = 2t/\tau_e$, where t is the optical wave round-trip time in the resonator. In order to achieve a high coupling, the phase match condition needs to be satisfied, i.e., the waveguide widths should be close at the coupling point. At the steady state with an incident wave of time dependency $e^{j\omega t}$, we have

$$s_t = \frac{j(\omega - \omega_0) + \frac{1}{\tau_l} - \frac{1}{\tau_e}}{j(\omega - \omega_0) + \frac{1}{\tau_l} + \frac{1}{\tau_e}}s_i. \tag{3}$$

The resonance has an inverse Lorentzian line shape. On resonance ($\omega = \omega_0$), the input normalized power transmission is

$$\left|\frac{s_t}{s_i}\right|^2 = \left|\frac{\tau_e - \tau_l}{\tau_e + \tau_l}\right|^2. \tag{4}$$

With critical coupling where the external delay rate is equal to the intrinsic delay rate, transmission reaches zero with an infinite ER [25]. The loaded Q-factor is given by

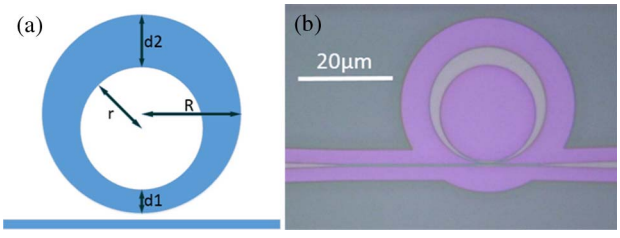

Fig. 1. (a) Schematic of the adiabatic microring resonator. (b) Microscope image of a typical adiabatic microring resonator with $R = 12$ μm, $r = 10$ μm, $d_1 = 0.35$ μm, and $d_2 = 1.65$ μm.

$$Q = \frac{\omega_0\tau}{2} = \frac{\omega_0}{2}\left(\frac{\tau_e\tau_l}{\tau_e + \tau_l}\right). \tag{5}$$

From the measured resonance Q-factor and ER, we can deduce the internal and external delay rates from Eqs. (4) and (5).

The resonance occurs when $\omega_0 t = 2m\pi$, where m ($m = 1, 2, 3, \ldots$) is the resonance azimuthal order number. As the ring waveguide width adiabatically changes, its effective refractive index is angle-dependent, and the round-trip time is given by an integral form,

$$t = \int_0^{2\pi} \frac{n_{\text{eff}}(\theta)R \cdot \mathrm{d}\theta}{c}, \tag{6}$$

where c is the light speed in vacuum. The resonance condition thus becomes

$$\frac{\omega_0}{c}R\int_0^{2\pi} n_{\text{eff}}(\theta)\mathrm{d}\theta = 2m\pi. \tag{7}$$

From the resonance frequency, we can get the average effective index:

$$\overline{n_{\text{eff}}} \equiv \frac{\int_0^{2\pi} n_{\text{eff}}(\theta)\mathrm{d}\theta}{2\pi} = \frac{mc}{\omega_0 R}. \tag{8}$$

The resonance free spectral range (FSR) $\Delta\omega$ is inversely proportional to the round-trip group delay τ_g as $\Delta\omega = 2\pi/\tau_g$. Therefore, we can derive the average group refractive index from the FSR:

$$\overline{n_g} \equiv \frac{\int_0^{2\pi} n_g(\theta)\mathrm{d}\theta}{2\pi} = \frac{c}{\Delta\omega R}. \tag{9}$$

3. EXPERIMENT AND ANALYSIS

We designed a group of adiabatic microring resonators with different inner hole radii and positions. We first fix d_1 at 0.35 μm and vary r to study its effect on the resonance spectrum. At the coupling point, the microring has an identical width with the bus waveguide, and hence the fundamental radial-order resonance mode could be efficiently excited. Figure 2 shows the measured normalized transmission spectra of transverse electric (TE) polarization for three inner radii. It is evident that strong resonances with a high ER are present for $r = 6$ μm while almost no discernable resonance dips are observed for $r = 10$ μm. At around 1510 nm, the resonance ER exceeds 36 dB for $r = 6$ μm, indicating the critical coupling is nearly satisfied with incoming light almost completely absorbed by the cavity. The resonator with $r = 6$ μm has a lower Q-factor than that of $r = 8$ μm, as shown in the inset.

Figures 3(a) and 3(b) show the delay rates as a function of wavelength for $r = 6$ and 8 μm extracted from Eqs. (4) and (5). Figures 3(c) and 3(d) show the effective and group refractive indices obtained from Eqs. (8) and (9). Around 1510 nm, the delay rates $1/\tau_l$ and $1/\tau_e$ intersect, indicating the critical coupling is satisfied. The device is at undercoupling and overcoupling before and after the intersection wavelength, respectively. When the inner circle radius is 8 um, the external decay rate exceeds the internal delay rate, leading to overcoupling. There are two main factors that affect the intrinsic decay rate. First, the roughness on sidewalls causes scattering loss due to the imperfect fabrication process. As a result, the resonance

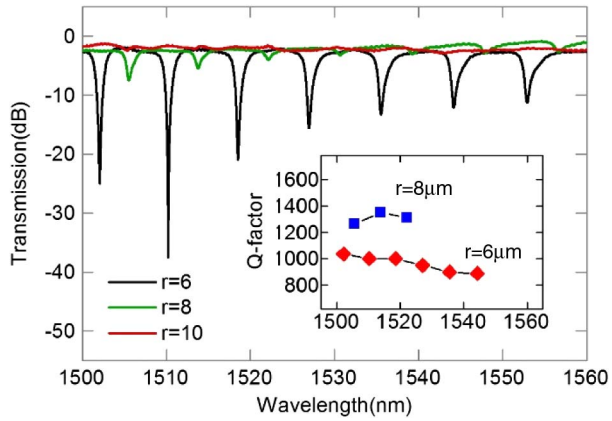

Fig. 2. Experimental transmission spectra of adiabatic microring resonators with $r = 6$, 8, and 10 μm and $d_1 = 0.35$ μm. The inset shows the Q-factor versus wavelength for $r = 6$ and 8 μm.

mode with more overlap with the sidewalls suffers a higher loss. Second, light transmission from the narrow waveguide section to the wide waveguide section causes mode transform loss. A slower adiabatic transform favors a lower loss. These two factors are in opposite trend as the inner radius increases. The measurement indicates that the resonator with $r = 8$ μm has a lower intrinsic decay rate than that of $r = 6$ μm, suggesting the transform loss plays the leading role. The external decay rate increases with wavelength because of the lower confinement at a longer wavelength.

According to Eq. (5), in order to get a high Q-factor, $1/\tau_l$ and $1/\tau_e$ should be lowered. As discussed above, the intrinsic decay rate $1/\tau_l$ is reduced when the ring waveguide is transformed more slowly. Therefore, we can increase the inner radius r and reduce the width difference $|d_1 - d_2|$ to make light propagate more smoothly in the ring waveguide. A low external decay rate results when the width difference between the bus waveguide and the ring waveguide becomes larger at the coupling point due to the phase mismatch.

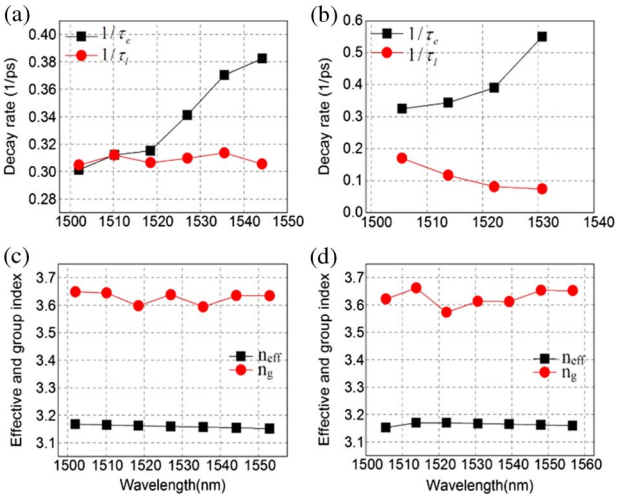

Fig. 3. Extracted device parameters from the measured spetra. (a) and (c): $r = 6$ μm; (b) and (d): $r = 8$ μm.

Therefore, we designed another two adiabatic ring resonators with $d_1 = 1.01$ and 2.99 μm to study their resonance properties. The inner radius is increased to $r = 8$ μm, and the bus waveguide width keeps the same at 0.35 μm. These two rings are essentially identical except for the coupling from the two opposite points. As the ring waveguide at the coupling region becomes wider, it could support multimodes. Figure 4(a) shows the modal dispersion curves of the narrowest ring waveguide section, together with the bus waveguide. The 1.01-μm-wide curved waveguide supports three TE modes with their effective indices higher than that of the bus waveguide, leading to a low $1/\tau_e$. Figure 4(b) depicts the electric-field profiles of the three modes at 1550 nm. Figure 4(c) shows the modal dispersion curves of the widest ring waveguide section. The 2.99-μm-wide waveguide supports up to six TE modes. The higher-order modes have effective indices closer to the bus waveguide mode, indicating they could be more easily excited. The modal profiles of the six modes are shown in Fig. 4(d). The mode profile of the straight bus waveguide is shown in Fig. 4(e) for comparison.

We then simulated light propagation in the adiabatic ring waveguide to obtain the mode transform loss. Figure 5 shows the electric-field intensity patterns in a half-ring computed using the 3D finite-difference time-domain (FDTD) simulation. Light with TE0 (fundamental), TE1 (first-order) and TE2 (second-order) modes is launched from the narrow waveguide section. The optical field at the wide waveguide section is analyzed and the conversion efficiency is obtained by overlap integral with the eigenmodes of the wide waveguide. Table 1 shows the conversion loss for each mode. It can be seen that the three modes suffer very low loss after half-ring transmission. Intermode mixing is also below −20 dB. Excitation of higher-order modes (TE3–TE5) is negligible (≤30 dB). Table 2 shows

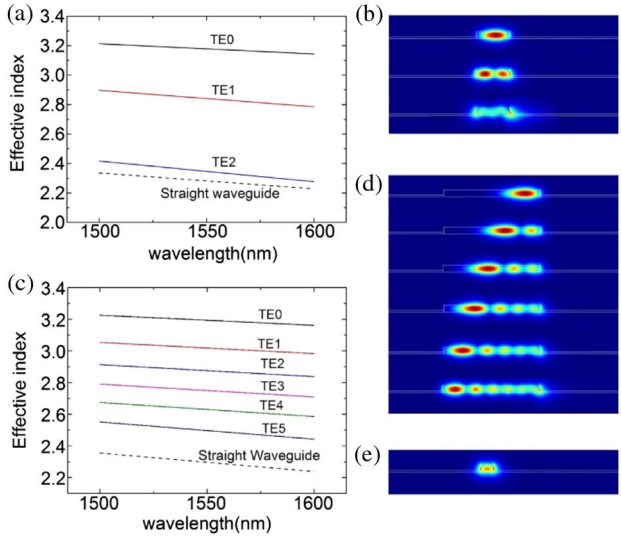

Fig. 4. (a) Effective indices of the three TE modes for the narrow ring waveguide with a width of 1.01 μm. (b) Electric-field profiles of the three TE modes for the narrow ring waveguide. (c) Effective indices of the six TE modes for the wide ring waveguide with a width of 2.99 μm. (d) Electric-field profiles of the six TE modes for the wide ring waveguide. (e) Electric-field profile of the fundamental mode for the bus waveguide.

Table 1. Simulated Transmission from the Narrow to the Wide Waveguide Section in a Half-Adiabatic Ring

	Output (dB)					
Input	TE0	TE1	TE2	TE3	TE4	TE5
TE0	−0.04	−21.16	−35.85	−37.34	−49.61	−57.83
TE1	−22.24	−0.16	−19.84	−31.13	−34.94	−36.67
TE2	−46.28	−28.38	−0.01	−22.56	−36.55	−42.35

the conversion loss when light is launched from the wide waveguide section. As expected, the modes TE3–TE5 cannot pass through as they are cut off in the narrow waveguide. Therefore, the adiabatic ring resonator only possesses three radial order modes, determined by the narrow waveguide section.

Figure 6 shows the experimental transmission spectra of the above two complementary adiabatic ring resonators. Two resonance modes can be clearly discerned from both resonators. The Q-factor reaches 1.3×10^5 for the resonator with $d_1 = 2.99$ μm. It is improved by 2 orders compared to the result shown in Fig. 2. It is also 1 order larger than that of the regular ring resonator fabricated using the same process. As both $1/\tau_l$ and $1/\tau_e$ are small, the exact critical coupling condition is hard to satisfy, leading to a lower extinction ratio. The inset shows the zoom-in view of the spectrum. Compared to TE2, TE1 is difficult to be excited because of the larger effective index difference, so TE1 has a lower $1/\tau_e$. In addition, because TE1 is less overlapped with the inner sidewall than TE2, it has a lower $1/\tau_l$. Both of the factors lead to a higher Q-factor for the TE1 mode. The effective index of the TE1 mode at the coupling point decreases for the other resonator with $d_1 = 1.01$ μm, leading to a larger $1/\tau_e$. As $1/\tau_l$ keeps the same, the larger mismatch between $1/\tau_l$ and $1/\tau_e$ results in a reduced extinction ratio. As for TE2, both $1/\tau_l$ and $1/\tau_e$ are high, so the Q-factor is low. TE0 has the largest effective index and is hence most difficult to be excited and we cannot observe the resonance dips in the spectrum.

It is interesting to see from the spectrum that TE1 is well aligned while TE2 is slightly misaligned by 0.9 nm for these two resonators. It could be caused by the geometric error in patterning these two separate resonators. From the modal profile, we see that TE2 has its optical power localized more inward than the TE1 mode. A slight deviation of the inner radius will shift TE2 more than TE1.

We also measured a reference microdisk resonator with the same outer radius to compare our adiabatic microring resonator. Figure 7 shows the experimental transmission spectrum of the microdisk resonator. Six resonance modes can be clearly discerned from the spectrum. Compared to Fig. 6, our adiabatic ring has only two modes with the other four modes fully rejected. It demonstrates the effectiveness of the adiabatic ring design in suppression high-order modes.

Table 2. Simulated Transmission from the Wide to the Narrow Waveguide Section in a Half-Adiabatic Ring

	Output (dB)		
Input	TE0	TE1	TE2
TE0	−0.04	−22.51	−26.82
TE1	−21.13	−0.22	−28.27
TE2	−35.56	−19.12	−0.07
TE3	−41.12	−30.82	−22.98
TE4	−40.88	−54.31	−36.72

As for our adiabatic ring resonator with $d_1 = 2.99$ μm, the group delay response measurement shows that TE1/TE2 has a positive/negative group delay, which suggests TE1/TE2 is overcoupled/undercoupled. It implies that $1/\tau_e > 1/\tau_l$ for the TE1 mode and $1/\tau_e < 1/\tau_l$ for the TE2 mode. In order to further enhance TE1 and suppress TE2, one approach is to increase the gap separation between the bus waveguide and the resonator. In this case, the external decay rates for both modes are reduced, making TE1 approach closer to critical coupling while TE2 more undercoupling. Hence, a quasi-single mode resonance could be obtained.

According to the above analyses, the design procedure for the waveguide-coupled adiabatic ring resonator is summarized as follows:

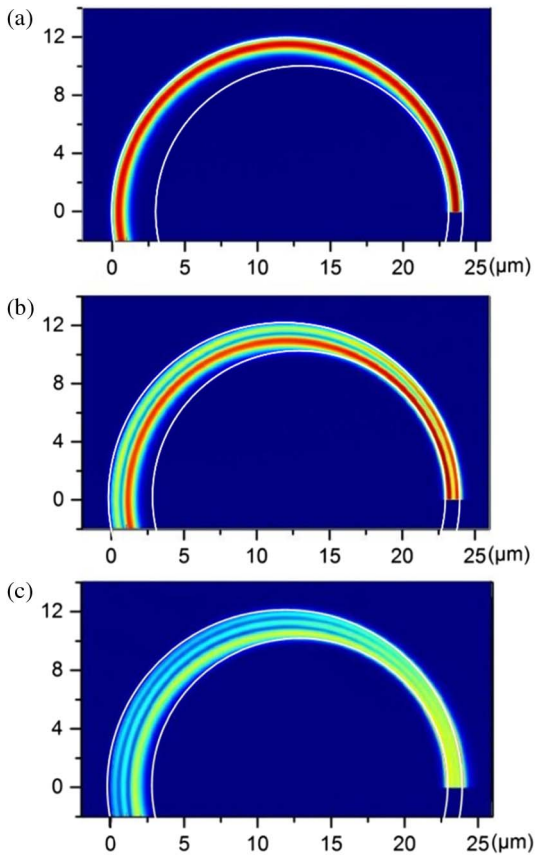

Fig. 5. Electric field intensity patterns computed using 3D FDTD when (a) TE0, (b) TE1, and (c) TE2 modes are excited at the input narrow waveguide end.

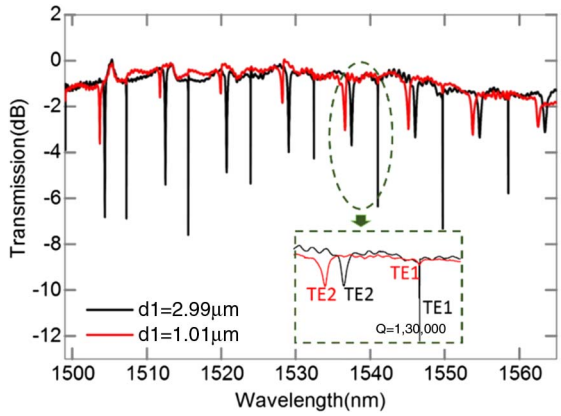

Fig. 6. Experimental transmission spectra for an adiabatic ring resonator when the bus waveguide is coupled from the narrowest and the widest ring wavguide sections.

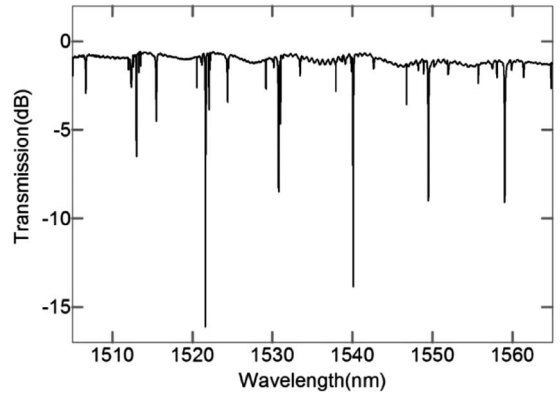

Fig. 7. Experimental transmission spectra of the microdisk with $R = 12$ μm.

1. Choose a proper ring outer radius R according to the required FSR.
2. Set d_1 so that only the first few resonance modes can be supported by the narrow ring waveguide.
3. Set d_2 to be large enough while ensuring the modal transform loss is negligible.
4. Calculate $1/\tau_l$ of the few resonance modes.
5. Design the bus waveguide width and gap separation to satisfy $1/\tau_e = 1/\tau_l$ for the resonance mode with the lowest loss.

It should be noted that generally $1/\tau_e = 1/\tau_l$ will not be satisfied for the other modes. For high-Q resonances, a slight discrepancy between $1/\tau_e$ and $1/\tau_l$ will make the resonance notch much shallower than the desired one. Therefore, the transmission spectrum will exhibit a quasi-single mode resonance.

4. CONCLUSION

We have demonstrated adiabatic ring resonators with few-mode high-Q resonances. Theoretical analysis reveals that the intrinsic and external decay rates both should be low and close in order to get high-Q and high-ER resonances. The intrinsic decay rate is determined by the modal round-trip loss. Two factors affects the intrinsic loss: the modal transform loss and the sidewall scattering loss. In order to lower the loss, the ring waveguide needs to be transformed slowly with reduced variation in width. The external decay rate is determined by the evanescent coupling between the ring and bus waveguide modes. Modal overlap and phase match are the two main factors affecting the coupling. The matched external coupling could be achieved by exciting a proper mode. The measurement of an adiabatic ring resonator with an outer radius $R = 12$ μm and a varying ring width from $d_1 = 1.01$ to 2.99 μm reveals it can excite two resonance modes with one possessing a high Q-factor of 1.3×10^5.

Funding. National Natural Science Foundation of China (NSFC) (61422508, 61535006); SRFDP of MOE (20130073130005); The 863 program (2013AA014402).

REFERENCES

1. J. R. Ong, R. Kumar, and S. Mookherjea, "Ultra-high-contrast and tunable-bandwidth filter using cascaded high-order silicon microring filters," IEEE Photonics Technol. Lett. **25**, 1543–1546 (2013).
2. F. N. Xia, M. Rooks, L. Sekaric, and Y. Vlasov, "Ultra-compact high order ring resonator filters using submicron silicon photonic wires for on-chip optical interconnects," Opt. Express **15**, 11934–11941 (2007).
3. L. Zhou, R. Soref, and J. Chen, "Wavelength-selective switching using double-ring resonators coupled by a three-waveguide directional coupler," Opt. Express **23**, 13488–13498 (2015).
4. P. Dong, S. Liao, D. Feng, H. Liang, D. Zheng, R. Shafiiha, C. C. Kung, W. Qian, G. Li, X. Zheng, A. V. Krishnamoorthy, and M. Asghari, "Low Vpp, ultralow-energy, compact, high-speed silicon electro-optic modulator," Opt. Express **17**, 22484–22490 (2009).
5. G. Li, A. V. Krishnamoorthy, I. Shubin, J. Yao, Y. Luo, H. Thacker, X. Zheng, K. Raj, and J. E. Cunningham, "Ring resonator modulators in silicon for interchip photonic links," IEEE J. Sel. Top. Quantum Electron. **19**, 95–113 (2013).
6. C. Ciminelli, F. Dell'Olio, D. Conteduca, C. M. Campanella, and M. N. Armenise, "High performance SOI microring resonator for biochemical sensing," Opt. Laser Technol. **59**, 60–67 (2014).
7. P. Orlandi, F. Morichetti, M. J. Strain, M. Sorel, P. Bassi, and A. Melloni, "Photonic integrated filter with widely tunable bandwidth," J. Lightwave Technol. **32**, 897–907 (2014).
8. D. Liang, M. Fiorentino, T. Okumura, H. H. Chang, D. T. Spencer, Y. H. Kuo, A. W. Fang, D. Dai, R. G. Beausoleil, and J. E. Bowers, "Electrically-pumped compact hybrid silicon microring lasers for optical interconnects," Opt. Express **17**, 20355–20364 (2009).
9. Q. Song, S. Liu, Z. Gu, N. Zhang, and S. Xiao, "Deformed microdisk coupled to a bus waveguide for applications in resonant filter," Opt. Lett. **39**, 1149–1152 (2014).
10. L. Qing, A. A. Eftekhar, P. Alipour, A. H. Atabaki, S. Yegnanarayanan, and A. Adibi, "Low-loss microdisk-based delay lines for narrowband optical filters," IEEE Photonics Technol. Lett. **24**, 1276–1278 (2012).
11. M. S. Rasras, K. Y. Tu, D. M. Gill, Y. K. Chen, A. E. White, S. S. Patel, A. Pomerene, D. Carothers, J. Beattie, M. Beals, J. Michel, and L. C. Kimerling, "Demonstration of a tunable microwave-photonic notch filter using low-loss silicon ring resonators," J. Lightwave Technol. **27**, 2105–2110 (2009).
12. S. M. Spillane, T. J. Kippenberg, and K. J. Vahala, "Ultralow-threshold Raman laser using a spherical dielectric microcavity," Nature **415**, 621–623 (2002).
13. W. Bogaerts, P. D. Heyn, T. V. Vaerenbergh, K. D. Vos, S. K. Selvaraja, T. Claes, P. Dumon, P. Bienstman, D. V. Thourhout, and R. Baets, "Silicon microring resonators," Laser Photonics Rev. **6**, 47–73 (2012).

14. J. Teng, P. Dumon, W. Bogaerts, H. Zhang, X. Jian, X. Han, M. Zhao, G. Morthier, and R. Baets, "Athermal silicon-on-insulator ring resonators by overlaying a polymer cladding on narrowed waveguides," Opt. Express **17**, 14627–14633 (2009).
15. M. Soltani, S. Yegnanarayanan, and A. Adibi, "Ultra-high Q planar silicon microdisk resonators for chip-scale silicon photonics," Opt. Express **15**, 4694–4704 (2007).
16. S. Xiao, M. H. Khan, H. Shen, and M. Qi, "Multiple-channel silicon micro-resonator based filters for WDM applications," Opt. Express **15**, 7489–7498 (2007).
17. M. S. Nawrocka, T. Liu, X. Wang, and R. R. Panepucci, "Tunable silicon microring resonator with wide free spectral range," Appl. Phys. Lett. **89**, 071110 (2006).
18. E. Shah Hosseini, S. Yegnanarayanan, A. H. Atabaki, M. Soltani, and A. Adibi, "Systematic design and fabrication of high-Q single-mode pulley-coupled planar silicon nitride microdisk resonators at visible wavelengths," Opt. Express **18**, 2127–2136 (2010).
19. M. Soltani, Q. Li, S. Yegnanarayanan, and A. Adibi, "Toward ultimate miniaturization of high Q silicon traveling-wave microresonators," Opt. Express **18**, 19541–19557 (2010).
20. X. Sun, K. Y. Fong, C. Xiong, W. H. Pernice, and H. X. Tang, "GHz optomechanical resonators with high mechanical Q factor in air," Opt. Express **19**, 22316–22321 (2011).
21. Z. Xia, A. A. Eftekhar, M. Soltani, B. Momeni, Q. Li, M. Chamanzar, S. Yegnanarayanan, and A. Adibi, "High resolution on-chip spectroscopy based on miniaturized microdonut resonators," Opt. Express **19**, 12356–12364 (2011).
22. R. Soref, J. Guo, and G. Sun, "Low-energy MOS depletion modulators in silicon-on-insulator micro-donut resonators coupled to bus waveguides," Opt. Express **19**, 18122–18134 (2011).
23. J. C. Mikkelsen, W. D. Sacher, and J. K. S. Poon, "Adiabatically widened silicon microrings for improved variation tolerance," Opt. Express **22**, 9659–9666 (2014).
24. B. E. Little, S. T. Chu, H. A. Haus, J. Foresi, and J. P. Laine, "Microring resonator channel dropping filters," J. Lightwave Technol. **15**, 998–1005 (1997).
25. A. Yariv, "Universal relations for coupling of optical power between microresonators and dielectric waveguides," Electron. Lett. **36**, 321–322 (2000).